Smart Structures and Systems, *Vol. 26*, *No. 6* (*2020*) *681-692*
DOI: https://doi.org/10.12989/sss.2020.26.6.681

Analytical and experimental investigation of stepped piezoelectric energy harvester

Deepesh Upadrashta[1], Li Xiangyang[1,2] and Yang Yaowen*[1]

[1]*School of Civil and Environmental Engineering, Nanyang Technological University, 50 Nanyang Avenue, 639798, Singapore*
[2]*Department of Astronautic Science and Mechanics, Harbin Institute of Technology, No.92 West Dazhi Street, Harbin 150001, China*

(*Received November 18, 2019, Revised September 21, 2020, Accepted September 28, 2020*)

Abstract. Conventional Piezoelectric Energy Harvesters (CPEH) have been extensively studied for maximizing their electrical output through material selection, geometric and structural optimization, and adoption of efficient interface circuits. In this paper, the performance of Stepped Piezoelectric Energy Harvester (SPEH) under harmonic base excitation is studied analytically, numerically and experimentally. The motivation is to compare the energy harvesting performance of CPEH and SPEHs with the same characteristics (resonant frequency). The results of this study challenge the notion of achieving higher voltage and power output through incorporation of geometric discontinuities such as step sections in the harvester beams. A CPEH consists of substrate material with a patch of piezoelectric material bonded over it and a tip mass at the free end to tune the resonant frequency. A SPEH is designed by introducing a step section near the root of substrate beam to induce higher dynamic strain for maximizing the electrical output. The incorporation of step section reduces the stiffness and consequently, a lower tip mass is used with SPEH to match the resonant frequency to that of CPEH. Moreover, the electromechanical coupling coefficient, forcing function and damping are significantly influenced because of the inclusion of step section, which consequently affects harvester's output. Three different configurations of SPEHs characterized by the same resonant frequency as that of CPEH are designed and analyzed using linear electromechanical model and their performances are compared. The variation of strain on the harvester beams is obtained using finite element analysis. The prototypes of CPEH and SPEHs are fabricated and experimentally tested. It is shown that the power output from SPEHs is lower than the CPEH. When the prototypes with resonant frequencies in the range of 56-56.5 Hz are tested at 1 m/s^2, three SPEHs generate power output of 482 μW, 424 μW and 228 μW when compared with 674 μW from CPEH. It is concluded that the advantage of increasing dynamic strain using step section is negated by increase in damping and decrease in forcing function. However, SPEHs show slightly better performance in terms of specific power and thus making them suitable for practical scenarios where the ratio of power to system mass is critical.

Keywords: stepped piezoelectric energy harvester; piezoelectricity; macro fiber composite; analytical modelling; finite element modelling

1. Introduction

Over the years, the design and development of self-powered Wireless Sensor Nodes (WSNs) and portable electronic devices for structural health and environmental monitoring, biomedical implants and military applications has garnered significant research focus. The recent advancements in integrated circuits and Microelectro-mechanical Systems (MEMS) have significantly reduced power consumption of electronic devices and provided impetus for realization of self-powered WSNs. The chemical batteries used for powering WSNs and low-power portable electronic devices are limited by their life span and energy density and their disposal causes environmental damage. Over the last decade, powering ultra-low power consuming electronic devices and WSNs using energy harvested from the ambient energy sources has attracted extensive research attention. These ambient energy sources that are suitable for energy harvesting, include solar, wind, thermal gradient and mechanical vibration energy. Vibration energy harvesting has gained huge attention because of its ubiquitous nature. Although there exist different transduction mechanisms for converting vibration-to-electricity such as electrostatic, electromagnetic, magneto-strictive etc., piezoelectric transduction has been preferred because of its high power density, high voltage output and ease of application (Roundy 2003, Cook-Chennault *et al*. 2008). Piezoelectric energy harvesting using ambient vibration sources has emerged as one of the promising solutions for replacing or recharging the batteries used in WSNs (Abdelkefi *et al*. 2014). The Conventional Piezoelectric Energy Harvesters (CPEHs) comprise a cantilever substrate beam and a layer of piezoelectric material is bonded partially or completely on one or both sides of the substrate beam. A tip mass is attached to the free end of the beam to tune the resonant frequency of the harvester to match the excitation frequency of vibration source. Numerous works have been carried out to maximize the performance of CPEHs in terms of voltage, power output, power density and efficiency using piezoelectric material selection, geometric, shape and structural

*Corresponding author, Ph.D., Professor,
E-mail: cywyang@ntu.edu.sg

ISSN: 1738-1584 (Print), 1738-1991 (Online)

optimization techniques, and using efficient electrical circuits. The electromechanical coefficient of piezoelectric materials directly influences the generated power output. Therefore, various materials such as Macro Fibre Composite (MFC) (Williams *et al*. 2002), polyvinylidene fluoride (Lee *et al*. 2005), AlN thin film (Marzencki *et al*. 2008), ZnO thin film (Ralib *et al*. 2012) and single crystal PMN-PT (Sun *et al*. 2009) have been developed to improve harvester's performance.

Many researchers have attempted to improve the performance of CPEHs by geometry modification and optimization of width, thickness and length dimensions of harvester beams and tip masses. Roundy *et al*. (2005) proposed triangular and trapezoidal cantilever beams to evenly distribute the strain over the length of beam to maximize the bending energy per unit volume of piezoelectric material. Hu *et al*. (2007) studied theoretically the performance of harvester beam with variable width and has shown that there exists an optimal inclination angle in the width to achieve maximum power density. A similar theoretical analysis was carried out by Dietl and Garcia (2010) to maximize the voltage output from long, slender beam with non-uniform width. Benasciutti *et al*. (2010) experimentally corroborated that higher power density can be achieved with trapezoidal shaped harvester when compared with conventional harvester. However, Matova *et al*. (2013) reported that the tapering of lateral profile of cantilever beams show positive effect on the performance of harvester only for long and slender beams but not for short and wide beams. A bio-inspired piezoelectric harvester with a trunk structure similar to an electric fish was proposed by Kim *et al*. (2014). PVDF film was used as piezoelectric material and the harvester produces 45% more power than the conventional harvester. Li *et al*. (2018) proposed a novel sandwich piezoelectric energy harvester with a soft core made of polycarbonate plastic and analyzed the harvesters' performance. The proposed sandwich harvester has a lower resonant frequency and generates a higher voltage output than the conventional harvester with the same geometrical dimensions. Izadgoshasb *et al*. (2019) designed and analyzed a multi-resonant piezoelectric energy harvester with two triangular shaped branches for achieving broadband energy harvesting at low-frequency vibrations. Design optimization was carried out on the geometry of the branches and tip masses to achieve two close resonant peaks in 1-10 Hz range. Cai and Harne (2019) carried out optimization of harvester design, geometry and nonlinearity to achieve enhanced dynamic performance. The study concludes that the trapezoidal beam shapes with monostable configuration are the best solution and the influence of tip mass is minimal as long as the beam shape, length and nonlinearity induced by magnets are appropriately chosen.

Paquin and St-Amant (2010) analytically investigated a piezoelectric harvester with varying thickness over the length and reported that the harvested power is increased by a factor of 3.6. Shafer *et al*. (2012a) optimized the thickness of piezoelectric layers relative to total beam thickness to achieve maximum power output while constraining system mass and resonant frequency. Wang *et al*. (2020) varied the thickness of substrate beam to achieve 78% higher energy harvesting efficiency. Upadrashta *et al*. (2015) varied the length of substrate beams to achieve higher power output from harvester while constraining the maximum strain on piezoelectric material below the allowable limit. Few researchers have attempted to improve the performance of harvesters through L-shaped (Li *et al*. 2010) and H-shaped (Guan *et al*. 2013) proof masses. Ma *et al*. (2016) proposed a novel design of proof mass based on a compliant mechanism to improve the harvester's performance. The harvester beam and proof mass are designed to achieve quadratic mode shape to achieve uniform strain over the harvester beam. The experiments have shown that the proposed design achieves two times the voltage output and four times the power output when compared with conventional harvester.

Several harvester designs with geometric discontinuities have been analyzed theoretically and experimentally to improve the harvester's voltage and power output. Since abrupt changes or discontinuities in the geometry induce increased stress/strain, geometric discontinuities such as step sections, cavities and irregular profiles have been introduced in the conventional harvester beam designs to increase the dynamic strain across the harvester beams under vibration, resulting in enhanced voltage and power output from the harvester. Čeponis *et al*. (2018) investigated the rectangular cantilever beams with irregular design of cross-sectional areas. The beam designs with cylindrical, rectangular and trapezoidal gaps have shown higher average strain than the conventional harvester. However, the resonant frequencies of beams with irregular profiles are much lower (105-125 Hz) when compared with conventional harvester (205 Hz). Under constant base acceleration, the harvesters vibrate under higher base displacements as the excitation frequency is reduced. A fair comparison requires harvesters characterized by same resonant frequency tested at same excitation amplitude. Usharani *et al*. (2017) studied a piezoelectric beam with a step section and an overhang length excited at the tip end. It is shown analytically and experimentally that a wide range of resonant frequencies can be achieved by changing the overhang length. It is also demonstrated that the harvester with step section generates three times more power than the conventional harvester. The same research group also investigated designs of stepped harvester with a cavity (Reddya *et al*. 2015) and a harvester with trapezoidal cavity (Reddy *et al*. 2015). It is worth noting that all the above proposed designs are excited at the tip with a harmonic force. When the same magnitude of tip force is applied on a conventional beam and a stepped beam, the latter undergoes higher deformation as it has low stiffness resulting in higher induced strain and consequently generates more power output than the conventional harvester. However, it is not practically easy to excite the piezoelectric harvester at the tip using ambient vibration sources. Most of the piezoelectric harvesters proposed in the literature are studied when excited by base vibration as it emulates the practical conditions more closely than the tip excitation. Therefore, the performance of stepped harvester is studied under base harmonic excitation in this work.

In this work, the performance of Stepped Piezoelectric

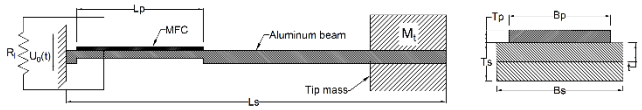

Fig. 1 (a) Schematic of stepped piezoelectric energy harvester under base excitation;
(b) harvester beam cross-section details

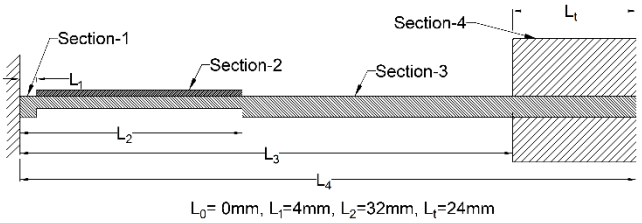

Fig. 2 Different segments of stepped harvester beam

Energy Harvester (SPEH) under base excitation is investigated using analytical and finite element models and experimentally as well. The motivation of study is to compare the energy harvesting performances of CPEH and SPEHs with same characteristics (resonant frequency) subject to harmonic base excitation. Previous studies compared the performances of CPEH and SPEHs with different resonant frequencies, which is not a fair comparison. In this study, CPEH and SPEHs with the same resonant frequency are designed and analyzed.

Firstly, a linear electromechanical model for analyzing both CPEH and SPEHs is presented. A finite element model of SPEH using commercial software ANSYS is also presented. Three configurations of SPEHs with same resonant frequency as that of CPEH are designed. The performance of harvesters in terms of open-circuit voltage, power output and specific power are evaluated analytically. Subsequently, the experimental results of harvester prototypes are presented and discussed. Finally, the accuracy of the analytical and finite element models is validated by comparing with experimental results and conclusions are given.

2. Stepped Piezoelectric Energy Harvester (SPEH)

Most of the piezoelectric harvesters adopt cantilever configuration for power generation from ambient vibration source. The cantilever structure can be attached to the vibration source as an add-on system and the resonant frequency can be tuned to the excitation frequency by proper selection of geometric parameters of the beam and tip mass. The proposed stepped piezoelectric harvester is shown in Fig. 1. A step is introduced in the substrate near to the clamped end of rectangular cantilever beam. In this study, Aluminium (Al-6065) is used as substrate material and a patch of piezoelectric Macro Fiber Composite (MFC) (model: M2814-P2; Smart Materials Corp.)[1] is bonded to the substrate beam over the step section. The MFC is chosen as piezoelectric material as it offers better conformability and provides reliable performance over long periods of time. Upadrashta and Yang (2016) studied the performance of MFC over 50 million of cycles and concluded that the performance of MFC is reliable under cyclic loading when the peak strain is below 800 με. A resistor (R_l) is connected across MFC to measure the electrical output. The energy harvesting circuit with a simple resistive load is chosen as the focus of study is comparison of the performances of CPEH and SPEHs.

2.1 Analytical modelling

A piezoelectric harvesting system is usually modelled as mass-spring-damper system with piezo element coupled between mechanical and electrical domains. Analytical modelling of piezoelectric harvesters under base excitation has been extensively studied in the literature and the open-circuit voltage, optimal resistance, power output and efficiency of harvesters have been thoroughly studied (Shu and Lien 2006a, b, Erturk and Inman 2009, Shafer and Garcia 2014). The governing electromechanical equations for the piezoelectric harvester under harmonic base excitation $u_0(t)$ are derived considering first-mode approximation and using the Hamiltonian principle and are given below. The influence of higher modes which are far away from first mode on the performance of harvesters is negligible and hence not considered

$$M\,\ddot{u}(t) + C\,\dot{u}(t) + K\,u(t) + \Theta\,V(t) = F(t) \tag{1}$$

$$\frac{V(t)}{R_l} + C^s\,\dot{V}(t) - \Theta\,\dot{u}(t) = 0 \tag{2}$$

where $u(t)$ is the modal mechanical amplitude in single mode approximation with displacement $w(x, t) = u(t)\emptyset(x)$; $\emptyset(x)$ is the mass normalized fundamental mode shape of the harvester beam. $V(t)$ is the voltage across the resistor R_l; M, K, C and Θ are the effective modal mass, stiffness, damping and electromechanical coupling terms, respectively, corresponding to the first mode $\emptyset(x)$; C^S is the clamped capacitance of MFC patch; and $F(t)$ is the external mechanical force due to the harmonic base excitation. The definitions of the above terms are given as below.

$$M = \int_0^{L_s} m_i(x)\,\emptyset(x)^2 dx \tag{3}$$

$$K = \int_0^{L_s} EI_i(x)\,\emptyset''(x)^2 dx \tag{4}$$

$$C = 2\xi\sqrt{KM} \tag{5}$$

$$\Theta = -\int_{v_p} y\emptyset''(x)\,e_{31}\psi(y)dv_p \tag{6}$$

$$F(t) = -\left(\int_0^{L_s} m_i(x)\,\emptyset(x)dx\right)\ddot{u}_0(t) \tag{7}$$

Here, m_i and EI_i are mass per unit length and flexural rigidity of i^{th} segment of the harvester beam as shown in Fig. 2. e31 is piezoelectric stress constant. The spatial

variable x is measured from the root and y is measured from the neutral axis of the beam. L, B and T represent length, width and thickness of harvester beams, respectively for substrate and piezoelectric beams represented using subscripts s and p. For instance, L_s is the length of the substrate beam. ξ is the damping ratio. The electric field over the MFC is defined by $\psi(y)$ and is assumed to be constant (Sodano *et al*. 2004). The integral in Eq. (6) to calculate electromechanical coupling coefficient is evaluated over the volume (vp) of MFC. The harvester beam is divided into four sections as show in Fig. 2 and the mode shape $\emptyset(x)$ is expressed for each segment as below.

$$\emptyset(x) = \emptyset_i(x) \quad \text{for} \quad L_{i-1} \le x \le L_i \quad \text{for} \quad i = 1 \text{ to } 4 \tag{8}$$

Differential eigenvalue problem for this configuration is

$$(EI)_i \emptyset_i^{iv} - m_i \omega^2 \emptyset_i = 0 \quad \text{for} \quad i = 1 \text{ to } 4 \tag{9}$$

The solution form for the mode shape is

$$\emptyset_i(x) = A_i cos(\beta_i x) + B_i sin(\beta_i x) + C_i cosh(\beta_i x) + D_i sinh(\beta_i x) \quad \text{for} \quad i = 1 \text{ to } 4 \tag{10}$$

with the following geometric and natural boundary conditions to determine the values of β_1, β_2, β_3 and β_4 which give non- trivial $\emptyset(x)$

$$\begin{cases} \emptyset_1(L_0) = 0, \quad \emptyset_1'(L_0) = 0 \\ \emptyset_i(L_i) = \emptyset_{i+1}(L_i), \quad \emptyset_i'(L_i) = \emptyset_{i+1}'(L_i) \text{ for } i = 1 \text{ to } 3 \\ (EI)_i \emptyset_i''(L_i) = (EI)_{i+1} \emptyset_{i+1}''(L_i) \quad \text{for } i = 1 \text{ to } 3 \\ (EI)_i \emptyset_i'''(L_i) = (EI)_{i+1} \emptyset_{i+1}'''(L_i) \quad \text{for } i = 1 \text{ to } 3 \\ (EI)_4 \emptyset_4''(L_4) = 0, \quad (EI)_4 \emptyset_4'''(L_4) = 0 \end{cases} \tag{11}$$

The rotational inertia of the tip mass is neglected as its influence is minimal. The coefficient matrix can be obtained by subjecting Eq. (10) to boundary conditions as given in Eq. (11). The eigenvalues of the system are calculated using the singularity condition of the coefficient matrix. Although the system has infinite eigenvalues corresponding to infinite natural modes of vibration, the fundamental eigenvalue and the first mode shape are considered in this study. The constants in Eq. (10) are determined and the derived mode shape is used for evaluating the system parameters required to solve governing Eqs. (1) and (2).

2.2 Finite element modelling

The analytical model gives accurate predictions of the output voltage and power from harvesters. However, the strain distribution and variation in different directions is complex in case of SPEH. Therefore, 3D finite element modelling using commercial software is opted to understand the strain distribution and its variation along the three directions of SPEH beam. Few studies have used commercially available finite element packages for studying the performance of linear and nonlinear piezoelectric harvesters (Abdelkefi *et al*. 2014, Upadrashta and Yang 2015, Yang and Upadrashta 2016).

The developed 3D finite element meshed model is shown in Fig. 3. The substrate beam and tip mass made of Aluminium are modelled with SOLID 186 element having three translational degrees of freedom (DOF). The MFC patch bonded on the step section is modelled with SOLID 226 element which is a coupled-field solid element. SOLID 226 has additional DOFs such as temperature and electric potential along with three structural DOFs. The element has the capability to simulate coupled structural-thermal-electric dynamic analyses. The elements of MFC are connected across a resistor (1 MΩ) element to evaluate the electrical output under dynamic loading. The beam is constrained at the clamped end by assigning zero displacement. Mesh convergence study is carried out by gradually increasing the number of elements in the three directions of harvester beam until convergence in the natural frequency, open-circuit voltage and tip displacement are achieved as shown in Table 1. The mesh size indicates the number of elements in the length, width and thickness directions of harvester beam. It can be observed from the tabulated data that beyond mesh size of 40 × 10 × 9, minimal change is observed in the results of finite element analysis with further mesh refinement and hence mesh size 40 × 10 × 9 is used for analyzing the harvester. The performance of harvester under base excitation is evaluated using harmonic analysis by sweeping the excitation frequency at constant base amplitude of 1 m/s^2. The results from both analytical model and finite element model are presented in the following section.

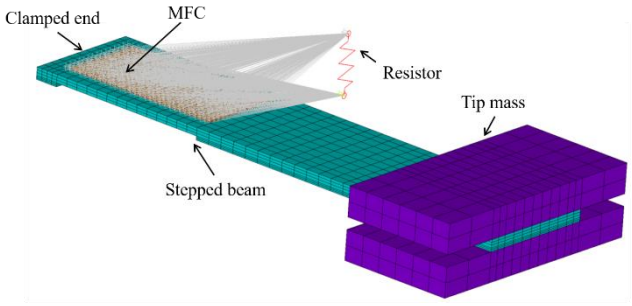

Fig. 3 3D Finite element model of stepped piezoelectric energy harvester

2.3 Analytical and finite element analysis results and discussion

The inclusion of step section reduces the stiffness of harvester beam and changes the mode shape of the beam in the step section. The electromechanical coupling coefficient depends on the slope change of the mode shape (Eq. (6)) and is consequently influenced by the presence of step. The influence of step section and tip mass value on the coupling coefficient is shown in Fig. 4. In this work, the ratio of thickness of substrate at step section (t) to the thickness over the other sections (T_s) is considered to distinguish various configurations of SPEHs. t/T_s ratio of 1 signifies that the harvester resembles CPEH without any step. Lower ratio of t/T_s indicates that the thickness of substrate at step section is less when compared with thickness at other sections of the beam. It can be inferred from the Fig. 4 that

Table 1 Influence of finite element model mesh size on the piezoelectric harvester's output

Mesh size	Natural frequency (Hz)	Peak open-circuit voltage (V_{rms})	Peak tip displacement (mm)
5 × 3 × 3	56.631	13.232	1.3687
10 × 5 × 3	56.14	13.116	1.3857
20 × 10 × 6	56.034	13.073	1.3955
40 × 10 × 6	56.002	12.997	1.3964
40 × 10 × 9	56	12.985	1.3957
40 × 20 × 12	56	12.976	1.3953
50 × 20 × 12	56	12.957	1.3951

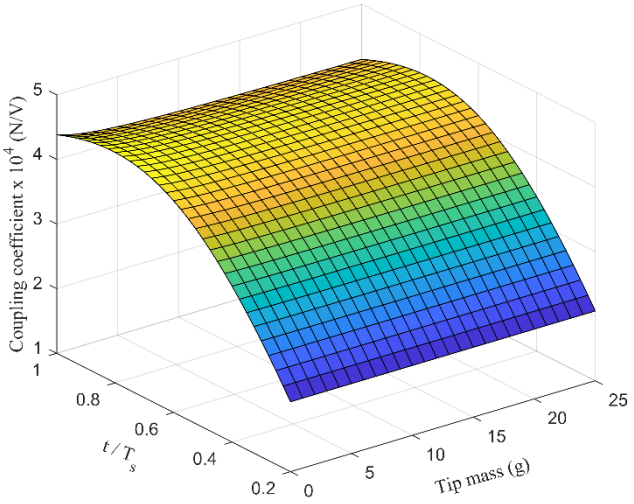

Fig. 4 Variation of electro-mechanical coupling coefficient with step thickness and tip mass

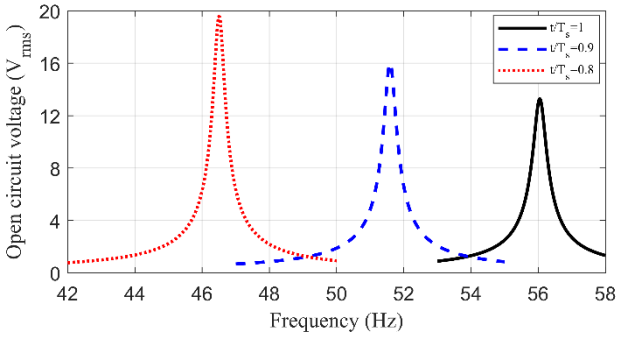

Fig. 5 Open-circuit voltage output from SPEHs with different step thickness at harmonic base excitation of 1 m/s^2

the coupling coefficient can be modified by introducing the step in the harvester beam. The value of coupling coefficient is increased initially with introduction of the step and then gradually decreased. However, the influence of tip mass value on the coupling coefficient is minimal. For a given step thickness ratio, the coupling coefficient is decreased slightly with increase of the tip mass. The results show that an optimal step thickness can be chosen to design

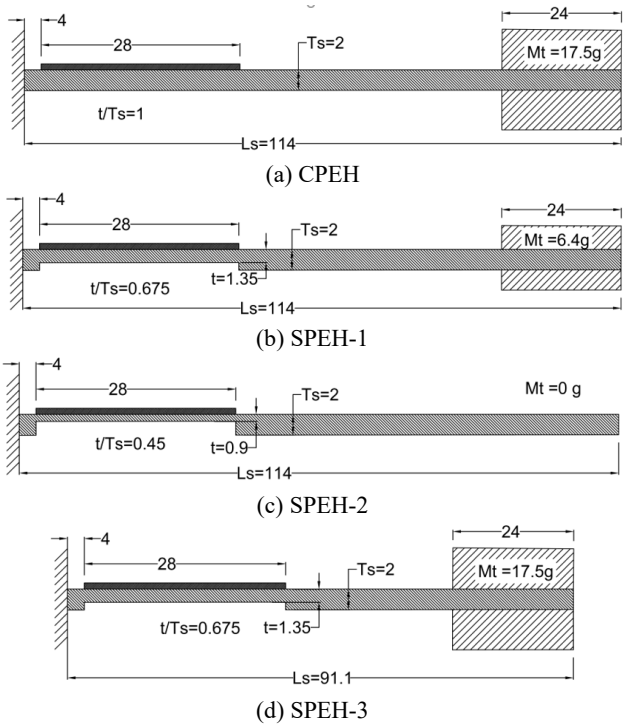

Fig. 6 The schematic diagrams of (a) CPEH; (b) SPEH-1; (c) SPEH-2; (d) SPEH-3

SPEH with better coupling coefficient than CPEH.

However, the inclusion of step section reduces the stiffness of the beam and consequently resonant frequency. The influence of step section on the performance of harvesters is shown in Fig. 5. As it is evident from figure, the resonant frequency of SPEH reduces accompanied by increase in maximum open-circuit voltage with decrease of step ratio. However, the increase in open circuit voltage at resonance is not solely attributed to step section but also increase in base amplitude (displacement) at lower excitation frequencies. When the harvesters are tested at constant base acceleration, they are subjected to higher base amplitudes as the excitation frequency reduces because the base amplitude is inversely proportional to square of excitation frequency ($Z_{amp} = Z_{acc} / \omega^2 \text{ Cos } (\omega t)$). Therefore, at a constant acceleration, higher base amplitudes are induced at lower excitation frequencies. In short, increase in voltage output from SPEHs is resulted from both geometric discontinuity (step section) and increase in base amplitude with reduction in resonant frequency. Therefore, for a fair comparison, both CPEH and SPEHs need to be designed with the same resonant frequency.

In this study, the performances of one configuration of CPEH and three different configurations of SPEHs are compared. The schematics of CPEH and SPEHs considered for the study are shown in Fig. 6. The resonant frequencies of harvesters are tuned to 56 Hz by varying the step thickness, tip mass and length of the beam. Note that the width and length of the step section and MFC patch are same for all configurations. In Fig. 7(a), the variation of resonant frequency of harvesters with tip mass (M_t) for fixed beam length (L_s = 114 mm) for three chosen t/T_s ratios is shown. Ratio t/T_s = 1 corresponds to harvesters without

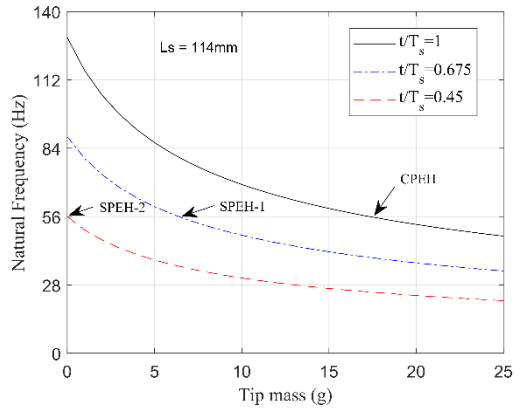

(a)

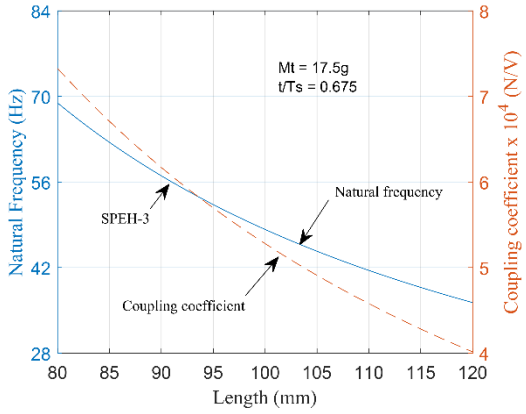

(b)

Fig. 7 (a) Variation of resonant frequency with tip mass for step thickness ratios 1, 0.675 and 0.45; (b) variation of resonant frequency and coupling coefficient with beam length for SPEH with step thickness ratio 0.675

step and the resonant frequency of 56 Hz is achieved with 17.5 g of tip mass. This design will be referred as CPEH in this work hereafter. It is evident from Fig. 7(a) that the stepped harvester requires lower tip mass values to achieve same resonant frequency as they have lower stiffness when compared with conventional harvester. For stepped harvester with t/T_s = 0.675, a tip mass of 6.4 g is required to achieve resonant frequency of 56 Hz and this design will be referred as SPEH-1. When t/T_s ratio is 0.45, the stepped harvester SPEH-2 achieves 56 Hz resonant frequency without any tip mass. Another configuration of stepped harvester with matched resonant frequency is achieved by reducing the length of the beam instead of reducing tip mass as shown in Fig. 7(b). SPEH-3 is designed with t/T_s = 0.675, M_t = 17.5 g and L_s = 91.1 mm. The reduction in length of beam also improves coupling coefficient as shown in figure. All the geometric and system parameters of one CPEH and three SPEH designs are given in Table 2. The material properties of Aluminium and MFC are given in Table 3.

Table 3 Material properties of piezoelectric energy harvesters

Parameter	Substrate	Piezoelectric
Material	Aluminium 6065	MFC M2814-P2
Elastic modulus (GPa)	69.5	30.336
Poisson's ratio	0.33	0.31
Density (kg/m^3)	2700	5440
Piezoelectric constant (C/m^2)	-	-5.16
Capacitance (nF)	-	30.8

It can be observed from the data in Table 2 that SPEH-3 design achieves better coupling coefficient than other designs through step section and reduction in length. Another noticeable observation is that SPEH-2 achieves same resonant frequency as others without tip mass but the coupling coefficient value is significantly reduced. The damping coefficient for each configuration is measured experimentally using logarithmic decrement method. It can be seen that the damping ratio is higher for stepped harvesters. The performances of harvesters are evaluated at harmonic base excitation of 1 m/s^2. The open-circuit voltage output from harvesters at 1MΩ load resistance is shown in Fig. 8(a). Open-circuit voltage is the maximum voltage that the harvester generates and is used conventionally as performance metric for comparing different designs of piezoelectric harvesters. It is evident from Fig. 8(a) that the

Table 2 Geometric and system parameters of piezoelectric harvesters

Parameter	CPEH	SPEH-1	SPEH-2	SPEH-3
t/T_s	1	0.675	0.45	0.675
Tip mass, M_t (g)	17.5	6.4	0	17.5
System mass (g)	30.5	18.14	10.87	26.78
$L_s \times B_s \times T_s$(mm^3)	114 × 20 × 2	114 × 20 × 2	114 × 20 × 2	91.1 × 20 × 2
$L_p \times B_p \times T_p$ (mm^3)	28 × 14 × 0.3	28 × 14 × 0.3	28 × 14 × 0.3	28 × 14 × 0.3
M (kg)	0.016449	0.008413	0.003525	0.01549
K (N/m)	2033.91	1040.23	436.02	1915.45
C (Ns/m)	0.116	0.059	0.248	0.109
Θ (N/V)	4.156E-4	4.367E-4	3.68E-4	6.06E-4
Damping ratio (%)	0.34	0.38	0.42	0.55

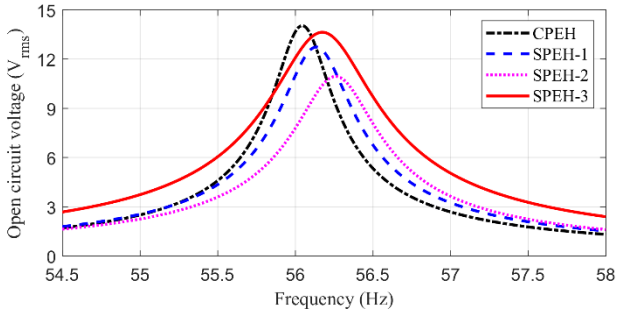

(a)

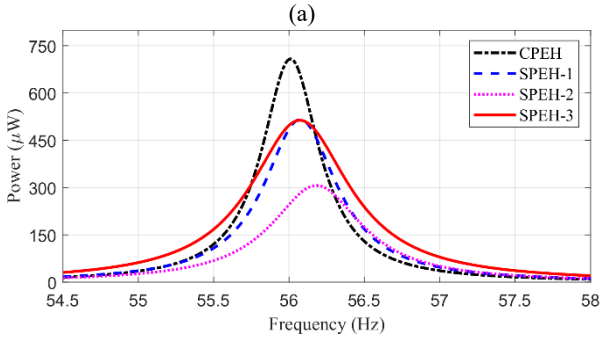

(b)

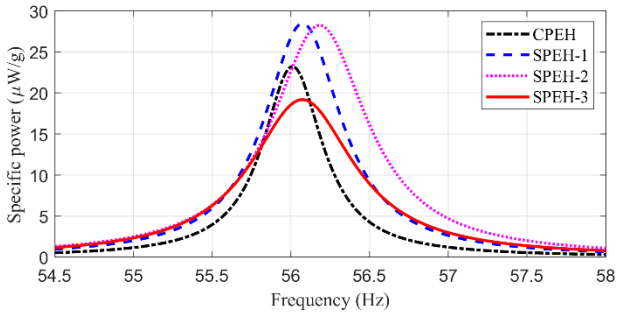

(c)

Fig. 8 (a) Analytical open-circuit voltage; (b) power output; (c) specific power frequency response functions of piezoelectric harvesters at base excitation of 1 m/s^2

SPEHs do not show improved performance when compared with CPEH. SPEH-3 generates voltage output approximately similar to CPEH. However, SPEH-1 and SPEH-2 generates lower voltage output than CPEH. The power output from harvesters at their optimal resistance values is shown in Fig. 8(b). The optimal load resistance values for CPEH, SPEH-1, 2 and 3 are 100 kΩ, 120 kΩ, 145 kΩ and 105 kΩ, respectively. The power output is calculated as $P_{out} = {V_{rms}^2}/{R_l}$. As it is evident from figure that CPEH generates maximum power output than all SPEHs. However, SPEH designs are useful when power to system mass ratio is a design constraint. For instances, stepped harvesters are useful in avian bio-logging (Shafer *et al.* 2012b) and harvesting from human limb motion (Renaud *et al.* 2009) applications where the harvested power needs to be maximized with constrains on device mass and size. Even in MEMS applications, the geometric discontinuities can be introduced to achieve the target frequency with lower dimensions (Sharpes *et al.* 2015). The specific power i.e., the ratio of power to system mass for

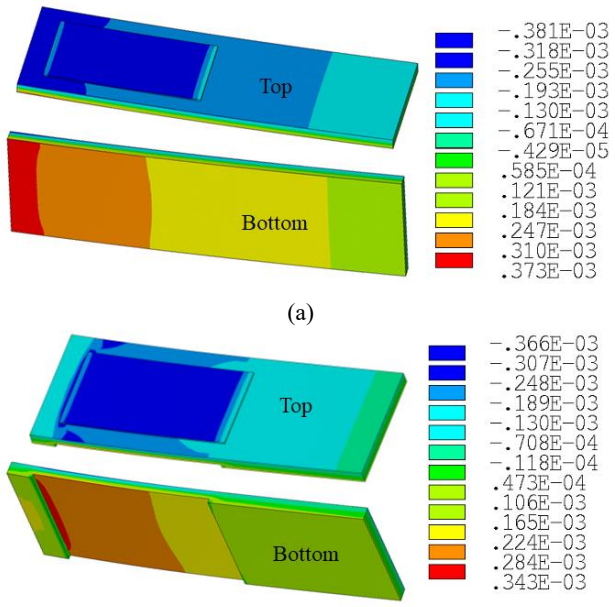

(a)

(b)

Fig. 9 Strain profile on top and bottom surfaces of (a) CPEH; (b) SPEH-3 beams at resonance

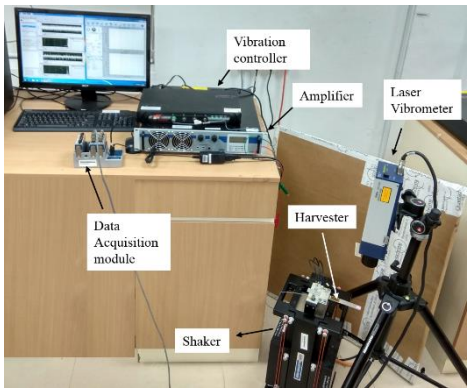

(a)

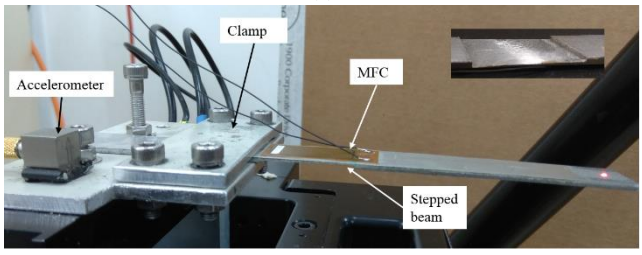

(b)

Fig. 10 (a) Experimental setup; (b) stepped piezoelectric energy harvester

different harvester configurations is shown in Fig. 8(c). System mass is the total mass of substrate beam, MFC and tip mass. SPEH-1 and SPEH-2 designs with lower tip masses show much better performance than CPEH and SPEH-3.

The performance of harvesters is influenced by multiple factors such as system mass, coupling coefficient and damping. CPEH has highest system mass, comparable

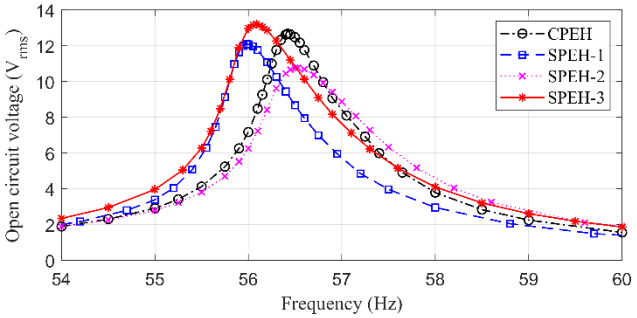

Fig. 11 Experimental open-circuit voltage frequency response functions of piezoelectric harvesters at base excitation of 1 m/s^2

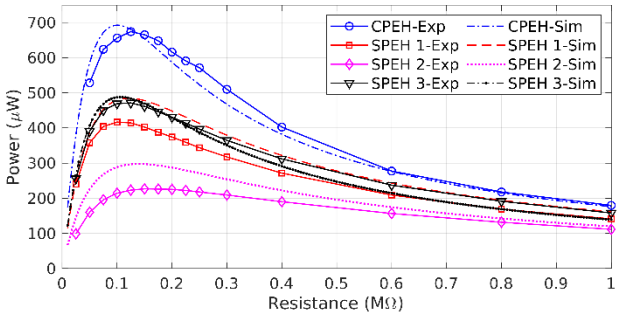

Fig. 12 Results of optimal resistance test from experiments and analytical model

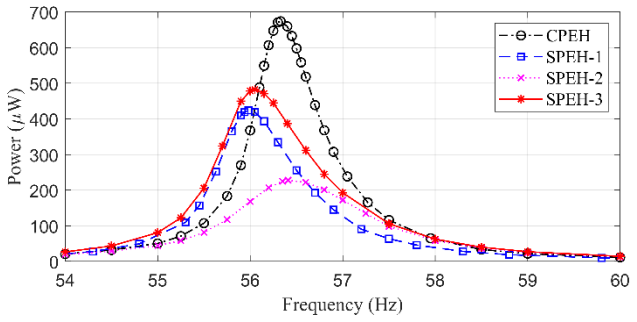

(a)

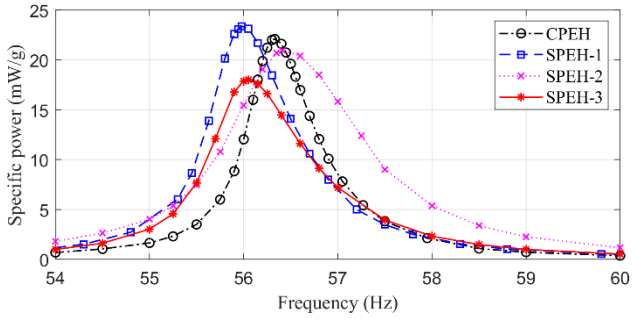

(b)

Fig. 13 (a) Experimental power output; (b) specific power output frequency response functions of piezoelectric harvesters at base excitation of 1 m/s^2

coupling coefficient and least damping and these factors combinedly resulted in better performance in terms of open-

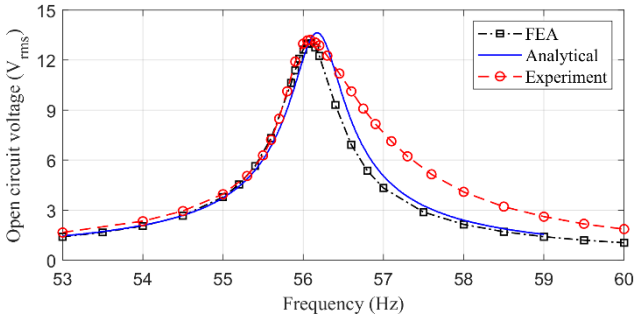

(a)

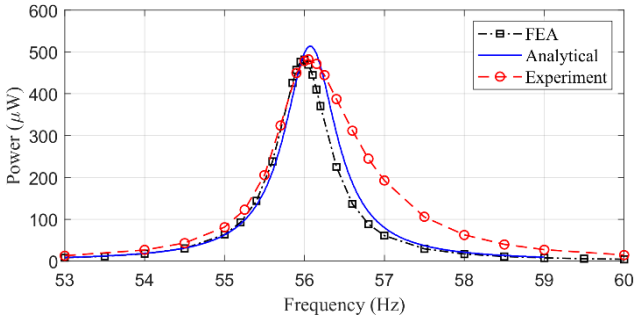

(b)

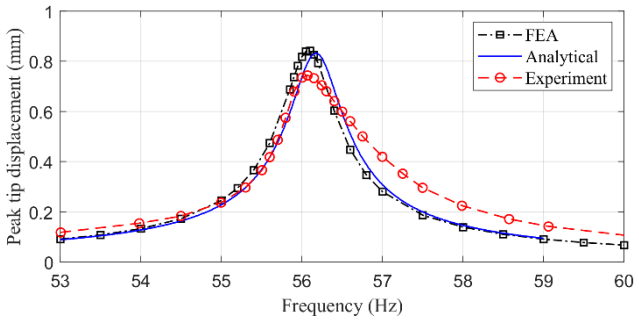

(c)

Fig. 14 Comparison among analytical, finite element model predictions and experimental results of SPEH-3 (a) open-circuit voltage; (b) power output; (c) tip displacement frequency response functions

circuit voltage and power output. The tip mass influences the magnitude of harmonic forcing function (Eq. (7)). Heavier tip mass increases the external force due to base vibration on the harvester and hence higher power output is achieved. However, heavier tip mass adversely affects the specific power as shown in Fig. 8(c).

SPEH-1 shows inferior performance mainly due to lower tip mass value and increased damping. Moreover, the coupling coefficient didn't increase significantly due to the incorporation of step in the harvester beam. SPEH-2 has no tip mass and hence the magnitude of harmonic force on the harvester is minimum and consequently, generates lower voltage and power output. Furthermore, the coupling coefficient decreased because of step incorporation and the damping is increased. However, SPEH-1 and SPEH-2 show better performance in terms of specific power because of the reduced tip mass. SPEH-3 design has maximum coupling coefficient and higher system mass when compared with CPEH and other SPEH configurations.

Table 4 Performance metrics of piezoelectric energy harvesters

Parameter	CPEH	SPEH-1	SPEH-2	SPEH-3
Resonant frequency (Hz)	56.33	55.98	56.53	56.05
Tip mass (g)	17.5	6.4	0	17.5
Total system mass (g)	30.5	18.14	10.87	26.78
Maximum open-circuit voltage (V_{rms})	12.67	12.1	10.77	13.21
Optimal load resistance (kΩ)	125	100	150	125
Maximum power output (μW)	674	424	228	482
Specific power (μW/g)	22.1	23.4	20.9	18.01
Damping ratio (%)	0.34	0.38	0.42	0.55

However, its performance is mitigated by higher damping resulting in lower open-circuit voltage and power output.

Damping in structures is a complex phenomenon and it depends on various factors such as material, geometry, displacement/deformation amplitude, stress/strain amplitude, stress gradient, frequency, hysteresis etc. In general, the damping increases with increase in stress amplitude in the vibrating structures (Gounaris *et al.* 2007). Colakoglu (2004) experimentally and numerically investigated the influence of frequency, amplitude of strain and temperature on the internal damping in the Aluminium alloys. The study clearly shows increase in the damping as the strain amplitude increases. SPEH configurations experience higher stress at the step sections because of geometric discontinuity and also steep stress gradient in the thickness direction of step section and consequently higher damping. The shorter, wide and thick beams experience higher damping than longer, narrow and thin beams (Dayou *et al.* 2015, Upadrashta *et al*. 2015). The advantage of SPEH-3 design with higher coupling coefficient is severely mitigated by the substantial increase in the damping ratio. As evident from Table 2, SPEH-3 configuration which has the shortest harvester beam of all the designs experience highest damping and consequently generates lower power output than CPEH despite having highest coupling coefficient and higher tip mass.

It is practically not possible to verify the strain induced in the step sections. Hence, finite element modelling is opted to study the distribution of strain over the CPEH and SPEH beams. The bending strain profiles of CPEH and SPEH-3 harvester beams at their resonance obtained from nodal solution of finite element analysis performed with ANSYS software are plotted in Figs. 9(a) and (b), respectively. The strain variation on both top and bottom surfaces of the harvester beams are shown in the figure. The variation of strain in width direction is minimal. The induced strain in Aluminium and MFC is reducing from clamped end to the tip end. The strain variation is maximum in thickness direction specially near the step section. At resonance, SPEH-3 undergoes much lower tip displacement (0.84 mm) than the CPEH (1.39 mm). However, almost similar magnitude of strains is induced in Aluminium and MFC materials of both and CPEH and SPEH-3 designs. The higher strain in SPEH-3 with much less tip displacement is because of presence of geometric discontinuity. It should be noted that strain gradients induced in the step section of SPEH-3 is higher than CPEH because of the reduced thickness. Higher strains can be induced in the harvester materials by lowering step thickness. However, the structural integrity and the long-term reliability of the harvesters will be severely affected when materials operate at higher strains. Normally, substrate materials possess higher material strain/stress limits when compared to piezoelectric materials. Upadrashta and Yang (2016) observed that the performance of MFC drastically reduces when tested at strains above 1000 με. Therefore, it is crucial to design harvesters with maximum induced strain under material strength limits (Shafer and Garcia 2013, Upadrashta *et al.* 2015). In the next section, the experimental results from the prototypes of harvesters are presented and discussed.

3. Experimental results and validation

In this section, experimental results are presented to validate the analytical and finite element model predictions. The prototypes of CPEH and three SPEHs are fabricated and tested. The complete experimental setup is shown in Fig. 10(a). The harvesters are mounted on the rocking arm of the long-stroke electrodynamic shaker (APS113). The shaker is capable of emulating harmonic, transient, impulse and random forces in the frequency range 0-100 Hz. The current excitation to the shaker is provided through amplifier (APS125). The amplitude and frequency of excitation is given through vibration controller (VR9500) and monitored through Vibrationview software. The voltage output from harvesters is measured using NI-9229 and the tip displacement is monitored using Polytec laser vibrometer. The step in the aluminium beam is created using milling machine at 4mm away from the clamped end. The length of step section is same as the length of MFC patch (28 mm). MFC is bonded on the harvester beam using 3M DP-460 epoxy glue. Aluminium plates are used as tip mass and mounted on the free end of harvester beams.

Experimentally measured open-circuit voltage output from CPEH and SPEH designs are shown in Fig. 11. Although, keen effort has been made, it is very difficult to achieve matching resonant frequencies for all harvesters. The resonant frequencies of harvesters are achieved in the range of 55.98 to 56.53 Hz which is admissible. As predicted from analytical models, SPEHs do not show improvement in open-circuit voltage output when compared with CPEH. SPEH-1 and SPEH-2 generates 4.5% and 15% less voltage output than CPEH. SPEH-3 generates 13.2V_{rms} at resonance when compared with 12.7V_{rms} from CPEH. The damping ratio of all the harvester configurations are measured at their resonance using logarithmic decrement method. The measured damping ratios of CPEH, SPEH-1, 2 and 3 are 0.34, 0.38, 0.42 and 0.55%, respectively. The maximum increase in the damping (62%) when compared

with CPEH is observed for SPEH-3 for which length of the beam also reduced. However, stepped harvesters can achieve 85-104% voltage output as CPEH with much reduced tip masses (SPEH-1 and 2) and reduced device length (SPEH-3). The performance metrics of all the harvesters are given in Table-4 for better understanding.

The optimal resistance test is carried out for the harvesters at 1 m/s^2 and the comparison between experimental results and simulation predictions are shown in Fig. 12. The experimental optimal load resistance values for CPEH, SPEH-1, 2 and 3 are 125 kΩ, 100 kΩ, 150 kΩ and 125 kΩ, respectively matching closely with the analytical predictions 100 kΩ, 105 kΩ, 145 kΩ and 120 kΩ. CPEH shows steep reduction in the power output when the load resistance moved from optimal to higher values. Stepped harvesters especially with lower step thickness (SPEH-2) shows very less reduction in the power output at higher load resistances. The resistance is varied in the intervals of 25 kΩ in the experiments compared to 5 kΩ interval used in analytical predictions. The experimental peak power output of CPEH and SPEH-3 matches excellently with analytical predictions. However, the analytical prediction of power outputs of SPEH-1 and SPEH-2 shows 17% and 31% discrepancy with experimental results. It should be noted that the error in power output is square of the error in voltage output. For instance, the voltage output from SPEH-2 at optimal resistance from experiments and analytical predictions is 5.85 V and 6.56 V, respectively showing a discrepancy of 0.7 V which is admissible. There are various reasons for the slight discrepancy observed in the results. Although very keen effort is made in incorporating the step in the substrate beam using milling machine, there is approximately 0.05-0.1 mm variation in the thickness of step section over its length. The layer of glue to bond the MFC patch over the substrate beam is not considered in both the analytical and finite element models. Secondly, the values of material properties of both Aluminium 6065 and MFC2814-P2 are taken from data sheet for analytical modelling. However, these values are subjected to slight variation and cannot be validated. For instance, the capacitance of MFC patch is given as 30.8 nF[1]. However, the capacitance of MFC patches used in the study are varying in the range of 27-32 nF when tested with multimeter. Similarly, the elastic modulus of MFC (69.5 GPa) shows slight nonlinear behavior at low strains and it is not taken into account in this study (Upadrashta and Yang 2016). All the above factors combined with experimental error induced slight discrepancy between analytical predictions and the experimental results.

The power output frequency response of all the harvesters at their respective optimal load resistances is plotted in Fig. 13(a). The CPEH performs much better than all the stepped harvesters. CPEH generates power output of 674 μW while SPEH-1, 2 and 3 generate 424 μW, 228 μW and 482 μW, respectively. It can be observed that the lower step thickness resulted in lower power output. Lower damping ratio, better combination of coupling coefficient and system mass and good performance at lower load resistances enabled CPEH to harvest more power than stepped harvesters. The specific power output from all harvesters is plotted in Fig. 13(b). The SPEH-1 design performs slightly better than CPEH and significantly better than SPEH-2 and SPEH-3. The improvement in specific power from SPEH-1 over CPEH is not as significant as predicted using analytical model. The primary reason for this discrepancy is the slight over prediction of power output from analytical model.

Finally, the analytical model and finite element model predictions are validated with experimental results. The analytical, FEA predictions and experimental open-circuit voltage, power output and tip displacement of SPEH-3 are compared in Figs. 14(a), (b) and (c), respectively. The predictions from both the analytical model and finite element model show very good agreement with experimental results. In general, the analytical model slightly over predicts the harvester's performance when compared with experimental results. The maximum open-circuit voltage from harvester at resonance is $13.6V_{rms}$, $13V_{rms}$ and $13.2V_{rms}$ from the analytical, FEA model and experiments, respectively. The power output from harvester is also very well predicted by both analytical and FEA models. The analytical and FEA models predict peak tip displacements at resonance as 0.83 mm and 0.84 mm compared to experimental value of 0.74 mm. The slight unsymmetrical behavior observed in frequency response functions from experiments is due to the material nonlinearity of MFC at strains below 1000 με Upadrashta and Yang (2016). Normally, the shift in resonance frequency is observed when the harvester is tested at increasing base accelerations due to material nonlinearity. However, the present study focusses on the comparison of performances of conventional and stepped harvesters rather than the influence of material nonlinearity at higher base accelerations. It should also be noted that the geometric nonlinearities will influence the performance of harvesters only when the tip displacement to the beam length ratio is more than 10% (Yang and Upadrashta 2016). However, in the present study where the harvester is tested at 1 m/s^2, the peak tip displacement to beam length ratio is less than 1%. Therefore, the influence of both geometric and material nonlinearities can be neglected for analyzing the harvester. Only, the fundamental mode is used in the analytical modelling of the stepped harvesters as the higher modes are well separated from the first mode. The first three bending modes of SPEH-3 are observed at 56 Hz, 825 Hz and 2395 Hz, respectively. The higher modes are far away from the first mode and therefore, have negligible influence on the performance of harvester tested at the fundamental resonance. From these results, it can be concluded that the derived analytical model and finite element model predict the dynamic behavior of stepped harvester with good accuracy.

4. Conclusions

The performance of SPEHs has been studied analytically and experimentally and compared with the CPEH. It is shown that with the same resonant frequency of

CPEH and SPEHs, the introduction of geometric discontinuity actually results in reduction of peak power. The advantage of increasing the dynamic strain using step section at the root of harvester beam is negated by increase in damping and decrease in forcing function. However, SPEHs show better performance in achieving better power to total system mass ratio, i.e., specific power. The study indicates that SPEHs are suitable for applications such as bio-logging, energy harvesting from human motion and MEMS devices where system mass is of critical importance. In other scenarios where the system mass is not a critical constraint, CPEH offers better performance.

Analytical and finite element models have been developed for SPEHs. The influence of step section on the resonant frequency and coupling coefficient has been investigated. It is shown that the coupling coefficient can be increased by choosing optimal step thickness. The inclusion of step section reduces the stiffness of the beam, changes the mode shape of the harvester beam and influences the coupling coefficient. SPEHs are characterized by lower stiffness, hence their resonant frequency can be tuned to the target frequency with significantly lower tip masses as compared with CPEH. Three different configurations of SPEHs and one CPEH have been designed with the same resonant frequency and their performance under harmonic base excitation of 1 m/s^2 has been evaluated using analytical modeling and finite element simulation, and the findings have been validated with experiments. Contrary to the existing notion, CPEH outperforms SPEHs in terms of open-circuit voltage and power output. The reduction in the system mass and increase in the damping adversely affected the performance of SPEHs. The three SPEHs generated 85%, 95.5% and 104% of CPEH open-circuit voltage with 21%, 51% and 94% of system mass of CPEH. When tested at optimal load resistances, SPEHs generated significantly lower power output than CPEH. The three SPEHs generated power output of 424 μW, 228 μW and 482 μW when compared with 674 μW from CPEH. However, SPEHs exhibit better performance in terms of specific power.

Funding acknowledgments

This research received no specific grant from any funding agency in the public, commercial, or not-for-profit sectors.

Notes

[1]https://www.smart-material.com/MFC-product-P2.html (accessed on September 20, 2020)

References

Abdelkefi, A., Barsallo, N., Tang, L., Yang, Y. and Hajj, M.R. (2014), "Modeling, validation and performance of low-frequency piezoelectric energy harvesters", *J. Intell. Mater. Syst. Struct.*, **25**(12), 1429-1444. https://doi.org/10.1177%2F1045389X13507638.

Benasciutti, D., Moro, L., Zelenika, S. and Brusa, E. (2010), "Vibration energy scavenging via piezoelectric bimorphs of optimized shapes", *Microsyst. Technol.*, **16**(5), 657-668. https://doi.org/10.1007/s00542-009-1000-5.

Cai, W. and Harne, R.L. (2019), "Vibration energy harvesters with optimized geometry, design, and nonlinearity for robust direct current power delivery", *Smart Mater. Struct.*, **28**(7), 075040. https://doi.org/10.1088/1361-665X/ab2549.

Čeponis, A., Mažeika, D., Kulvietis, G. and Ying, Y. (2018), "Piezoelectric cantilevers for energy harvesting Wwith irregular design of the cross sections", *Mechanics*, **24**(2), 221-231. https://doi.org/10.5755/j01.mech.24.2.18019.

Colakoglu, M. (2004), "Factors effecting internal damping in aluminium", *J. Theor. Appl. Mech.*, **42**, 95-105.

Cook-Chennault, K., Thambi, N. and Sastry, A. (2008), "Powering MEMS portable devices-a review of non-regenerative and regenerative power supply systems with special emphasis on piezoelectric energy harvesting systems", *Smart Mater. Struct.*, **17**(4), 043001. https://doi.org/10.1088/0964-1726/17/4/043001.

Dayou, J., Kim, J., Im, J., Zhai, L., How, A.T.C. and Liew, W.Y. (2015), "The effects of width reduction on the damping of a cantilever beam and its application in increasing the harvesting power of piezoelectric energy harvester", *Smart Mater. Struct.*, **24**(4), 045006. https://doi.org/10.1088/0964-1726/24/4/045006.

Dietl, J.M. and Garcia, E. (2010), "Beam shape optimization for power harvesting", *J. Intell. Mater. Syst. Struct.*, **21**(6), 633-646. https://doi.org/10.1177%2F1045389X10365094.

Erturk, A. and Inman, D.J. (2009), "An experimentally validated bimorph cantilever model for piezoelectric energy harvesting from base excitations", *Smart Mater. Struct.*, **18**(2), 025009. https://doi.org/10.1088/0964-1726/18/2/025009.

Gounaris, G.D., Antonakakis, E. and Papadopoulos, C.A. (2007), "Hysteretic damping of structures vibrating at resonance: An iterative complex eigensolution method based on damping-stress relation", *Comput. Struct.*, **85**(23-24), 1858-1868. https://doi.org/10.1016/j.compstruc.2007.02.026.

Guan, Q.C., Ju, B., Xu, J.W., Liu, Y.B. and Feng, Z.H. (2013), "Improved strain distribution of cantilever piezoelectric energy harvesting devices using H-shaped proof masses", *J. Intell. Mater. Syst. Struct.*, **24**(9), 1059-1066. https://doi.org/10.1177%2F1045389X13476150.

Hu, H., Cui, Z. and Cao, J. (2007), "Performance of a piezoelectric bimorph harvester with variable width", *J. Mech.*, **23**(3), 197-202. https://doi.org/10.1017/S1727719100001222.

Izadgoshasb, I., Lim, Y.Y., Vasquez Padilla, R., Sedighi, M. and Novak, J.P. (2019), "Performance enhancement of a multiresonant piezoelectric energy harvester for low frequency vibrations", *Energies*, **12**(14), 2770. https://doi.org/10.3390/en12142770.

Kim, G.W., Kim, J. and Kim, J.H. (2014), "Flexible piezoelectric vibration energy harvester using a trunk-shaped beam structure inspired by an electric fish fin", *Int. J. Precis. Eng. Manuf.*, **15**(9), 1967-1971. https://doi.org/10.1007/s12541-014-0552-1.

Lee, C., Joo, J., Han, S., Lee, J. and Koh, S. (2005), "Poly (vinylidene fluoride) transducers with highly conducting poly (3, 4-ethylenedioxythiophene) electrodes," *Synth. Met.*, **152**(1-3), 49-52. https://doi.org/10.1016/j.synthmet.2005.07.116.

Li, W.G., He, S. and Yu, S. (2010), "Improving power density of a cantilever piezoelectric power harvester through a curved L-shaped proof mass", *IEEE Trans. Ind. Electron.*, **57**(3), 868-876. https://doi.org/10.1109/TIE.2009.2030761.

Li, X., Upadrashta, D., Yu, K. and Yang, Y. (2018), "Sandwich piezoelectric energy harvester: Analytical modeling and experimental validation", *Energy Convers. Manag.*, **176**, 69-85. https://doi.org/10.1016/j.enconman.2018.09.014.

Ma, X., Wilson, A., Rahn, C.D. and Trolier-McKinstry, S. (2016), "Efficient energy harvesting using piezoelectric compliant mechanisms: theory and experiment", *J. Vib. Acous.*, **138**(2),

021005. https://doi.org/10.1115/1.4032178.
Marzencki, M., Ammar, Y. and Basrour, S. (2008), "Integrated power harvesting system including a MEMS generator and a power management circuit", *Sens. Actuators A Phys.*, **145**, 363-370. https://doi.org/10.1016/j.sna.2007.10.073.
Matova, S., Renaud, M., Jambunathan, M., Goedbloed, M. and Van Schaijk, R. (2013), "Effect of length/width ratio of tapered beams on the performance of piezoelectric energy harvesters", *Smart Mater. Struct.*, **22**(7), 075015. https://doi.org/10.1088/0964-1726/22/7/075015.
Paquin, S. and St-Amant, Y. (2010), "Improving the performance of a piezoelectric energy harvester using a variable thickness beam", *Smart Mater. Struct.*, **19**(10), 105020. https://doi.org/10.1088/0964-1726/19/10/105020.
Ralib, A.A.M., Nordin, A.N., Salleh, H. and Othman, R. (2012), "Fabrication of aluminium doped zinc oxide piezoelectric thin film on a silicon substrate for piezoelectric MEMS energy harvesters", *Microsyst. Technol.*, **18**(11), 1761-1769. https://doi.org/10.1007/s00542-012-1550-9.
Reddy, A.R., Umapathy, M., Ezhilarasi, D. and Uma, G. (2015), "Cantilever beam with trapezoidal cavity for improved energy harvesting", *Int. J. Precis. Eng. Manuf.*, **16**(8), 1875-1881. https://doi.org/10.1007/s12541-015-0244-5.
Reddya, A.R., Umapathy, M., Ezhilarasib, D. and Uma, G. (2015), "Modelling and experimental investigations on stepped beam with cavity for energy harvesting", *Smart Struct. Syst., Int. J.*, **16**(4), 623-640. https://doi.org/10.12989/sss.2015.16.4.623.
Renaud, M., Fiorini, P., Van Schaijk, R. and Van Hoof, C. (2009), "Harvesting energy from the motion of human limbs: the design and analysis of an impact-based piezoelectric generator" *Smart Mater. Struct.*, **18**(3), 035001. https://doi.org/10.1088/0964-1726/18/3/035001.
Roundy, S.J. (2003), "Energy scavenging for wireless sensor nodes with a focus on vibration to electricity conversion", Ph.D. Dissertation, University of California, USA.
Roundy, S., Leland, E.S., Baker, J., Carleton, E., Reilly, E., Lai, E., Otis, B., Rabaey, J.M., Wright, P.K. and Sundararajan, V. (2005), "Improving power output for vibration-based energy scavengers", *IEEE Pervasive Comput.*, **4**(1), 28-36. https://doi.org/10.1109/MPRV.2005.14.
Shafer, M.W. and Garcia, E. (2013), "Fundamental power limits of piezoelectric energy harvesters based on material strength", *Prodeedings of the Active and Passive Smart Structures and Integrated Systems 2013, International Society for Optics and Photonics*, San Diego, USA, April.
Shafer, M.W. and Garcia, E. (2014), "The power and efficiency limits of piezoelectric energy harvesting", *J. Vib. Acous.*, **136**(2), 021007. https://doi.org/10.1115/1.4025996.
Shafer, M.W., Bryant, M. and Garcia, E. (2012a), "Designing maximum power output into piezoelectric energy harvesters", *Smart Mater. Struct.*, **21**(8), 085008. https://doi.org/10.1088/0964-1726/21/8/085008.
Shafer, M.W., Bryant, M. and Garcia, E. (2012b), "A practical power maximization design guide for piezoelectric energy harvesters inspired by avian bio-loggers", *Proceedings of the ASME 2012 Conference on Smart Materials, Adaptive Structures and Intelligent Systems, American Society of Mechanical Engineers*, Georgia, USA, September.
Sharpes, N., Abdelkefi, A. and Priya, S. (2015), "Two-dimensional concentrated-stress low-frequency piezoelectric vibration energy harvesters", *Appl. Phys. Lett.*, **107**(9), 093901. https://doi.org/10.1063/1.4929844.
Shu, Y.C. and Lien, I. (2006a), "Efficiency of energy conversion for a piezoelectric power harvesting system", *J. Micromech. Microeng.*, **16**(11), 2429. https://doi.org/10.1088/0960-1317/16/11/026.
Shu, Y. and Lien, I. (2006b), "Analysis of power output for piezoelectric energy harvesting systems", *Smart Mater. Struct.*, **15**(6), 1499. https://doi.org/10.1088/0964-1726/15/6/001.
Sodano, H.A., Park, G. and Inman, D. (2004), "Estimation of electric charge output for piezoelectric energy harvesting", *Strain*, **40**(2), 49-58. https://doi.org/10.1111/j.1475-1305.2004.00120.x.
Sun, C., Qin, L., Li, F. and Wang, Q.M. (2009), "Piezoelectric energy harvesting using single crystal Pb (Mg1/3Nb2/3) O_3-x$PbTiO_3$ (PMN-PT) device", *J. Intell. Mater. Syst. Struct.*, **20**(5), 559-568. https://doi.org/10.1177%2F1045389X08097385.
Upadrashta, D. and Yang, Y. (2015), "Finite element modeling of nonlinear piezoelectric energy harvesters with magnetic interaction", *Smart Mater. Struct.*, **24**(4), 045042. https://doi.org/10.1088/0964-1726/24/4/045042.
Upadrashta, D. and Yang, Y. (2016), "Experimental investigation of performance reliability of macro fiber composite for piezoelectric energy harvesting applications", *Sens. Actuator A Phys.*, **244**, 223-232. https://doi.org/10.1016/j.sna.2016.04.043.
Upadrashta, D., Yang, Y. and Tang, L. (2015), "Material strength consideration in the design optimization of nonlinear energy harvester", *J. Intell. Mater. Syst. Struct.*, **26**(15), 1980-1994. https://doi.org/10.1177%2F1045389X14546651.
Usharani, R., Uma, G., Umapathy, M. and Choi, S.B. (2017), "A new piezoelectric-patched cantilever beam with a step section for high performance of energy harvesting", *Sens. Actuator A Phys.*, **265**, 47-61. https://doi.org/10.1016/j.sna.2017.08.031.
Wang, B., Luo, X., Liu, Y. and Yang, Z. (2020), "Thickness-variable composite beams for vibration energy harvesting", *Compos. Struct.*, **2020**, 112232. https://doi.org/10.1016/j.compstruct.2020.112232.
Williams, R.B., Grimsley, B.W., Inman, D.J. and Wilkie, W.K. (2002), "Manufacturing and mechanics-based characterization of macro fiber composite actuators", *Proceedings of the ASME 2002 international mechanical engineering congress and exposition, American Society of Mechanical Engineers*, New Orleans, USA, November.
Yang, Y. and Upadrashta, D. (2016), "Modeling of geometric, material and damping nonlinearities in piezoelectric energy harvesters", *Nonlin. Dyn.* **84**(4), 2487-2504. https://doi.org/10.1007/s11071-016-2660-1.

HJ